J Nanostruct 14(2): 622-637, Spring 2024

RESEARCH PAPER

Synthesis, Characterization, and In Vivo Evaluation of Polyurethane-based Scaffolds Containing Graphene Oxide and Icariin for Bone Tissue Engineering

Baryham S. Abdul Samad, Nadia A. Al-Asady *

Department of Chemistry, College of Education for Pure Science, University of Bsarah, Basra, Iraq

ARTICLE INFO

Article History:
Received 06 January 2024
Accepted 25 March 2024
Published 01 April 2024

Keywords:
Degradation
Graphene oxide
Icariin
Nanoparticles
Porosity
Toluene diisocyanate scaffolds

ABSTRACT

In this work, porous scaffolds are based on polyurethane, with graphene oxide (GO) and Iiracin nanospheres. We fabricated scaffolds using Toluene diisocyanate and polyelectrolyte, incorporating graphene oxide and Icariin-loaded nanospheres, scaffolds were thoroughly characterized using various analytical techniques, including FTIR, XRD, H-NMR, ^{13}C NMR, and SEM. Decomposition patterns were evaluated in oxidizing and enzymatic settings, demonstrating steady disintegration across multiple weeks. The results of the in vivo analysis provided compelling evidence of their therapeutic potential, with both scaffold variants showing good biocompatibility in rabbit models, the TDI/GO/I scaffold particularly excelled, demonstrating enhanced bone regeneration and stable hematological profiles over the four-week implantation period, radiographic analysis revealed progressive bone formation, with significant defect closure observed by week three, while blood parameters remained within normal ranges throughout the study.

How to cite this article
Abdul Samad B., Al-Asady N. Synthesis, Characterization, and In Vivo Evaluation of Polyurethane-based Scaffolds Containing Graphene Oxide and Icariin for Bone Tissue Engineering. J Nanostruct, 2024; 14(2):622-637. DOI: 10.22052/JNS.2024.02.023

INTRODUCTION

The development of advanced biochemical materials for controlled drug delivery systems has garnered considerable interest in recent years because of their ability to improve therapeutic effectiveness while reducing side effects [1]. Polymer-based scaffolds emerged as promising candidates owing to their versatility, biocompatibility, and ability to modulate drug release kinetics [2]. Their intrinsic adaptability allows customization in form and function [3]. In addition, hydrogels improve their interaction with biological tissues, improving biocompatibility [4], while the profiles of grasping customized drugs improve therapeutic effectiveness [5].

Toluene diisocyanate TDI is a widely used precursor in polyurethane synthesis [6], and offers excellent mechanical properties and chemical versatility, making it an ideal choice for scaffold fabrication [7], the incorporation of graphene oxide GO, two-dimensional carbon nanomaterial, potentially enhance mechanical strength, electrical conductivity, and drug loading capacity of the scaffolds [8, 9]. Conversely, incorporating polyelectrolytes, polymers with ionizable groups, influences the scaffolds' surface characteristics and drug release kinetics. On the other hand, the integration of polyelectrolytes, which are polymers bearing ionizable groups, modulates the scaffolds' surface properties and drug-release behavior [10]. The first version of the scaffold system, consisting of TDI and GO, aims to utilize

* *Corresponding Author Email: nadia.hussein@uobasrah.edu.iq*

the unique features of graphene oxide to create a stable and flexible platform for drug delivery. The second system, combining TDI with PE, seeks to exploit the ionic interactions and swelling behavior of polyelectrolytes to achieve controlled release of therapeutic agents. Both scaffolds were loaded with Icariin (ICA) Fig. 1, a traditional Chinese medicine that was used to treat and prevent numerous health disorders, such as cardiovascular diseases, osteoporosis, or sexual dysfunction [4]. Recently, several studies investigated their potential as a drug against many common health issues. In some cases, their medicinal effects were greater than those of certain currently used drugs [5,6]. For example, in the case of Alzheimer's disease prevention, they have approximately the same efficacy as donepezil, but they are less toxic [7].

A new delivery system was investigated to increase the bone regeneration effect of ICA. This method resulted in higher efficiency in bone regeneration and repair.

Among various other factors, flavonoids' low bioavailability remains a major one. This study focuses on producing two novel scaffolds utilizing toluene diisocyanate and incorporating graphene oxide or polyelectrolyte (PE) as functional elements for controlled drug release and tissue engineering.

MATERIALS AND METHODS

Materials

Toluene diisocyanate $CH_3C_6H_3(NCO)_2$ (Sigma-Aldrich, USA, 99% purity). Hydroxyapatite (HA) ($Ca_5(PO_4)_3(OH)$), (Aldrich, USA, particle size <200 nm, ≥90% purity). Phosphate Buffer Solution (PBS) (LRCO). Ethylenediamine (EN) ($C_2H_8N_2$, Aldrich, USA). N,N'-Dimethylformamide (DMF) (C_3H_7NO, Fisher Chemical). Hydrogen Peroxide (H_2O_2, Aldrich, USA). Calcium Chloride (Fluka, USA, ≥97% purity). Poly Electrolyte (PE), obtained from reverse osmosis water treatment plants at the Petrochemical Company, Basra, Iraq. Icariin $C_{33}H_{40}O$ Graphene oxide.

Synthesis of Polymer Scaffolds

Preparation of Toluene with Graphene Oxide Scaffold and Drug-Loaded Nanospheres

The fabrication of the graphene oxide-incorporated toluene diisocyanate scaffold commenced with the preparation of a polymeric solution. Toluene diisocyanate (3 mL) was combined with polycaprolactone (1 g) in dimethylformamide (3 mL), and the mixture was homogenized using a magnetic stirrer for 60 minutes. Graphene oxide (0.3 g) was introduced into the solution and thoroughly dispersed. Followed by the addition of hydroxyapatite (0.2 g). The toluene diisocyanate mixture was then gradually introduced into the aqueous polyelectrolyte solution under constant agitation, to facilitate cross-linking, 3 drops diethylenetriamine and 2 drops triethylenetetramine were incorporated into the mixture, and the resulting composite solution was transferred into mold to generate porous polymeric scaffold structure.

Prior to the drying process, 0.1 g of Icariin-loaded nanospheres were uniformly distributed

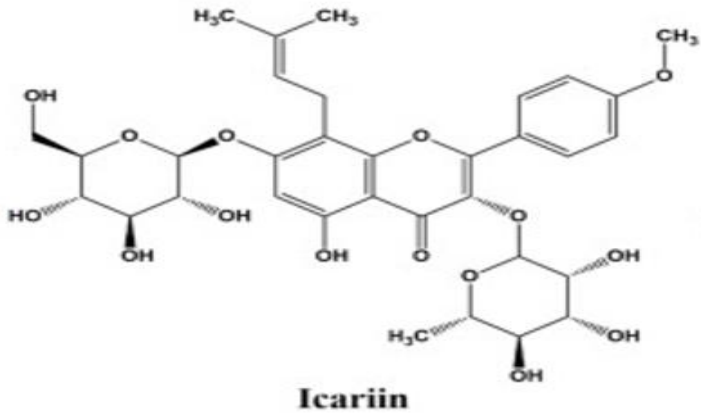

Fig. 1. The molecular structure of icariin

throughout the scaffold solution. These drug-laden nanospheres were previously synthesized using an ionotropic gelation technique involving sodium alginate and calcium chloride solutions.

Development of Polyelectrolyte-Enhanced Toluene Diisocyanate Scaffold

The synthesis of a polyelectrolyte-enhanced toluene diisocyanate scaffold began with the preparation of a polymeric blend. 3 mL of Toluene diisocyanate was mixed with 1.5 g of polycaprolactone and subjected to magnetic stirring for 60 min to ensure thorough blending. Subsequently, the solution comprising 0.3 g of hydroxyapatite dissolved in 2 mL of dimethylformamide was introduced to the mixture, along with 0.3 g beta-cyclodextrin. In a separate vessel, 0.5 g polyelectrolyte was dissolved in distilled water, the hydroxyapatite solution was then gradually incorporated into the aqueous polyelectrolyte solution under continuous agitation, and the toluene diisocyanate blend was slowly introduced into this polyelectrolyte mixture. To promote cross-linking, 3 drops diethylenetriamine and 2 drops triethylenetetramine were added to the composite solution, then the resulting mixture was cast into mold to form a porous polymeric scaffold.

Before initiating the drying process, Icariin-loaded nanospheres (0.1 g), previously prepared using an ionotropic gelation method involving sodium alginate and calcium chloride solutions, were evenly dispersed throughout the scaffold solution.

Both scaffold formulations were allowed to solidify and dry at ambient temperature, yielding the final composite structures for subsequent characterization and evaluation.

Surgical Implantation of Drug-Loaded Scaffolds in Rabbit Femoral Defects

Adult male rabbits (1800-2500g) were maintained under controlled conditions (25 ± 3°C; 40-50% humidity) with ad libitum access to food and water. Following two weeks of acclimatization, animals were randomly allocated into experimental groups. The study protocol was approved by the Ethics Committee at the University of Basra's College of Veterinary Medicine.

Surgical procedures were performed under aseptic conditions. Animals received prophylactic enrofloxacin (10 mg/kg, IM) pre-operatively. General anesthesia was induced using xylazine hydrochloride 2% (5mg/kg, IM) followed by ketamine hydrochloride 10% (35 mg/kg, IM) after 10 minutes. The lateral aspect of the thigh was prepared aseptically using standard protocols.

A 10-cm lateral skin incision was made along

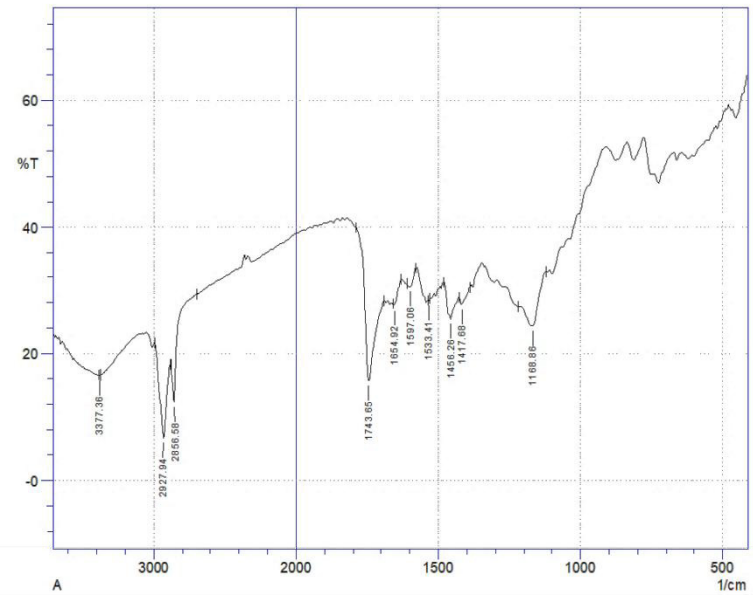

Fig. 2. The FTIR spectrum of the toluene with graphene oxide scaffold.

an imaginary line from the greater trochanter to the lateral patella. The fascia lata was sharply dissected, while vastus lateralis and biceps femoris muscles were bluntly separated to expose the femoral midshaft. A standardized 5mm diameter defect was created using a manual drill. After irrigation with sterile saline and hemostasis, defects were filled with 1g of the respective scaffold formulations.

Muscle layers and fascia were reconstructed using 3-0 polyglycolic acid in a simple continuous pattern, while skin closure was achieved with 3-0 silk sutures in an interrupted pattern. Post-operative care included systemic antibiotics (enrofloxacin 5%, 5 mg/kg, SC) and analgesics (meloxicam 0.2 mg/kg, SC) for five days. Healing progression was monitored through weekly radiographic examination, hematological analysis, and biochemical parameters over four weeks. Animals were humanely euthanized at designated time points for tissue collection and histopathological evaluation.

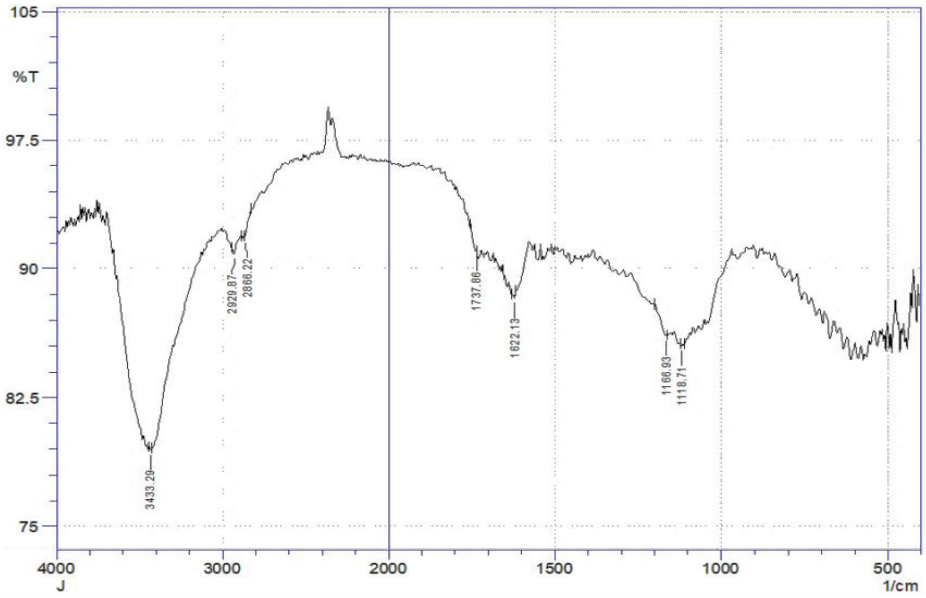

Fig. 3. FTIR spectrum of toluene diisocyanate with polyelectrolyte scaffold

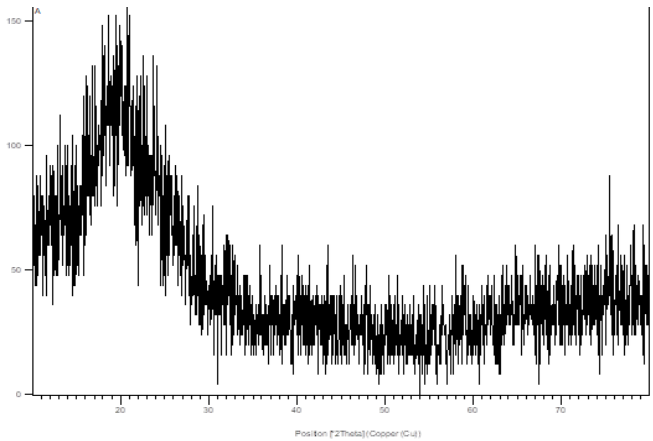

Fig. 4. XRD pattern of toluene with graphene oxide scaffold

RESULTS AND DISCUSSION

Structural and Chemical Characterization of Synthesized Scaffolds

Fourier-Transform Infrared Spectroscopic Analysis

Fourier-transform infrared (FTIR) spectroscopy was utilized to elucidate the chemical composition and identify functional groups within the synthesized scaffolds. This analytical technique was applied to the toluene diisocyanate-graphene oxide (TDI-GO) scaffold and the toluene diisocyanate-polyelectrolyte (TDI-PE) scaffold. The resulting FTIR spectra are presented in Figs. 2 and 3, respectively.

The FTIR spectrum of the TDI-GO scaffold (Fig. 2) revealed several distinctive absorption bands. A broad signal centered at 1168 cm^{-1} was attributed to C-O-C stretching vibrations in the epoxy groups of graphene oxide. The region between 1417-1654 cm^{-1} exhibited multiple broad peaks, indicative of aromatic C=C stretching modes. A sharp absorption at 1743 cm^{-1} corresponded to C=O stretching in isocyanate moieties. Two adjacent sharp peaks at 2856 and 2927 cm^{-1} were assigned to symmetric and asymmetric C-H stretching vibrations in methyl groups. Additionally, a broad band at 3377 cm^{-1} was observed, characteristic of O-H stretching in hydroxyl functionalities. These spectral features provide strong evidence for the successful integration of the toluene diisocyanate-based scaffold and graphene oxide sheets.

Analysis of the FTIR spectrum for the TDI-PE scaffold (Fig. 3) revealed several key absorption bands. Broad, low-intensity signals at 1118 and 1166 cm^{-1} were attributed to C-O stretching vibrations in ether and ester groups. A prominent broad peak at 1622 cm^{-1}, accompanied by a less intense signal at 1737 cm^{-1}, corresponded to aromatic C=C and C=O stretching in isocyanate functionalities. Minor peaks at 2866 and 2929 cm^{-1} were assigned to C-H stretching vibrations in methyl groups. A broad, high-intensity band centered at 3433 cm^{-1} was indicative of N-H stretching in amine and amide moieties. These spectral observations confirm the successful incorporation of toluene diisocyanate into the polyelectrolyte matrix, the presence of broad, overlapping peaks suggests the formation of hydrogen bonding interactions between scaffold components, which influences the material's physicochemical properties.

X-ray Diffraction Analysis

X-ray diffraction (XRD) studies were performed to elucidate the crystalline structure and phase composition of the synthesized scaffolds. The resulting diffractograms are presented in Figs. 3 and 4 for the toluene diisocyanate-graphene oxide (TDI-GO) and toluene diisocyanate-polyelectrolyte (TDI-PE) scaffolds, respectively.

Examination of the XRD pattern for the TDI-GO scaffold (Fig. 4) revealed a series of distinctive diffraction peaks. The most prominent reflection was observed at 2θ = 20.88°, corresponding to an interplanar spacing of 4.26 Å. This peak is characteristic of the (002) crystallographic plane of graphene oxide, providing strong evidence for the successful integration of GO sheets within the scaffold matrix, additional reflections were

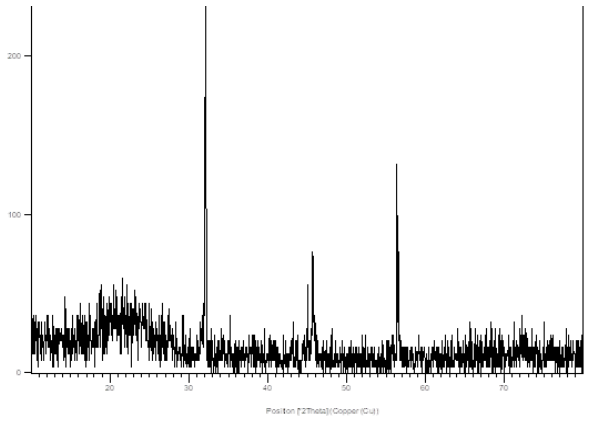

Fig. 5. XRD pattern of toluene diisocyanate with polyelectrolyte scaffold

identified at 2θ values of 10.66°, 21.81° and 63.98°. These peaks are associated with crystalline domains of polyurethane components, which form as a result of the reaction between toluene diisocyanate, and polycaprolactone during scaffold synthesis.

Analysis of the XRD pattern for the TDI-PE scaffold (Fig. 5) unveiled several notable diffraction peaks. A high-intensity reflection was observed at 2θ = 32.12°, exhibiting a d-spacing of 2.79 Å. This peak is attributed to the crystalline regions of the polyurethane component within the scaffold. The diffractogram also displayed additional reflections at 2θ values of 18.87°, 45.04°, 46.73°, and 56.40°, these peaks are indicative of the presence and distribution of the polyelectrolyte component throughout the scaffold matrix.

The XRD analysis provides crucial insights into the structural organization, and phase composition of the fabricated scaffolds, the observed diffraction patterns corroborate the successful incorporation of graphene oxide and polyelectrolyte components to their respective scaffold matrices, the presence of peaks associated with polyurethane crystalline domains in both scaffolds confirms the formation of the desired polymeric network. These findings collectively demonstrate successful synthesis of the targeted scaffold systems, by crystalline features consistent with the expected structural components.

Scanning Electron Microscopy Analysis

We elucidate the morphological features and microstructural characteristics of the synthesized scaffolds by employing scanning electron microscopy (SEM), the micrographs obtained

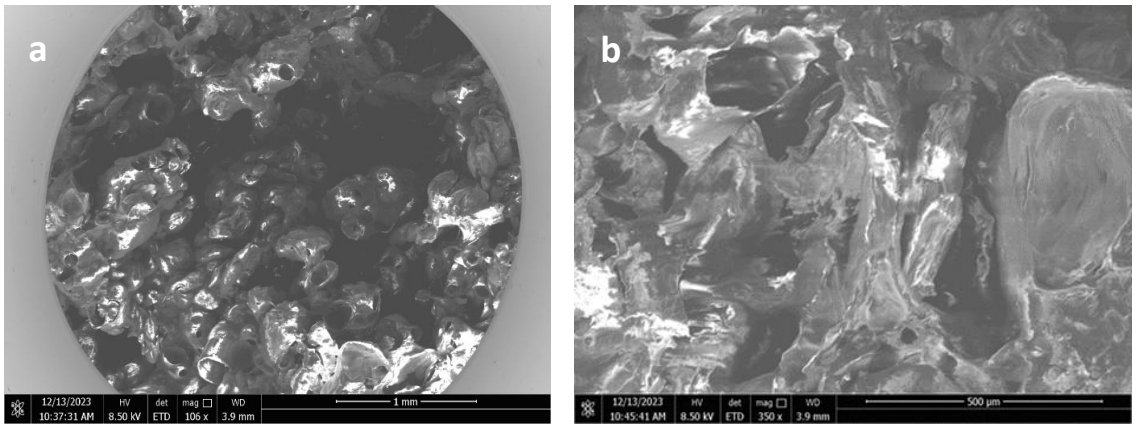

Fig. 6. SEM images of toluene with graphene oxide scaffold

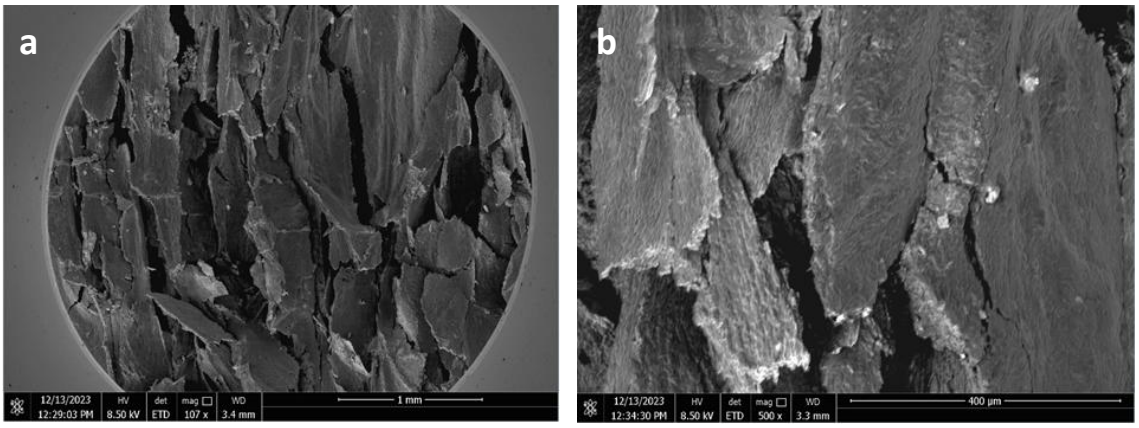

Fig. 7. SEM images of toluene diisocyanate scaffold with polyelectrolyte

revealed distinct architectural properties of each scaffold composition.

Fig. 6 presents the SEM images of the toluene diisocyanate-graphene oxide (TDI-GO) scaffold. The micrographs unveil a complex three-dimensional network characterized by interconnected, sheet-like structures, these structures exhibit irregular shapes with wrinkled surfaces and tend to form clustered arrangements. The scaffold's architecture is marked by a high degree of porosity, featuring a multitude of cavities and openings of varying dimensions. This arrangement results in a randomly oriented, interconnected network of platelets, creating an irregular yet highly porous

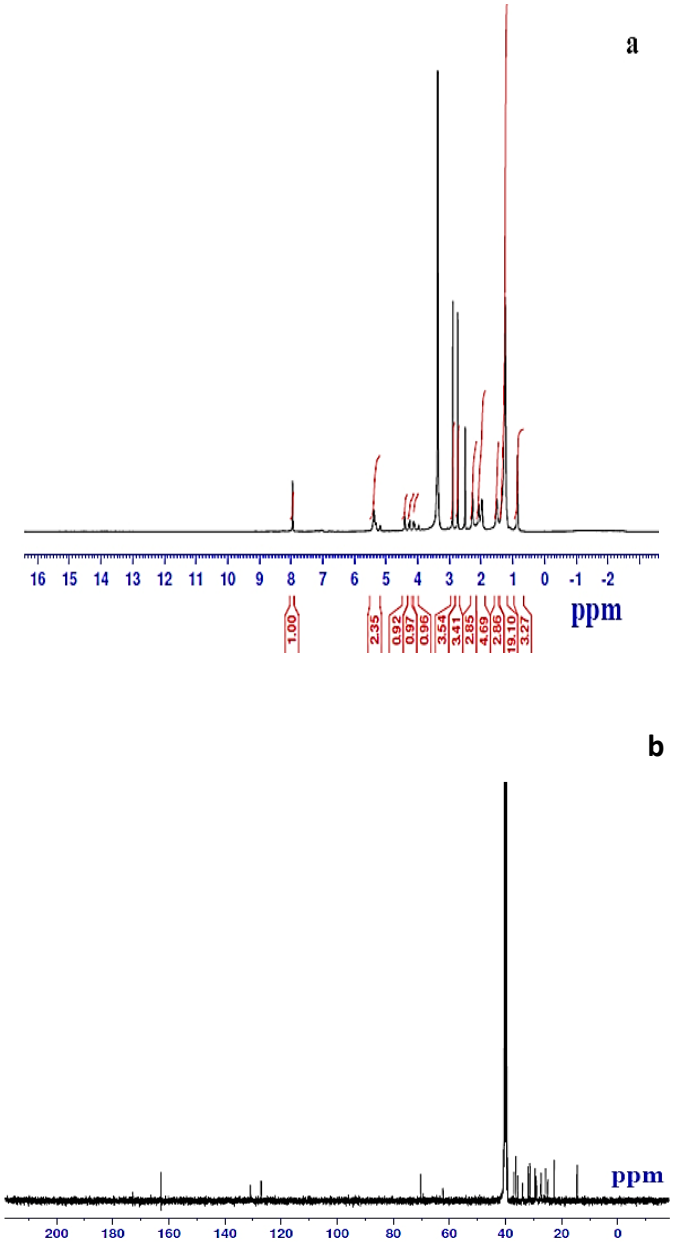

Fig. 8. a) X - 1H NMR spectrum of toluene with graphene oxide scaffold b) Y - ^{13}C NMR spectrum of toluene with graphene oxide scaffold

structure by a wide distribution of pore sizes throughout the material.

The morphological features of the toluene diisocyanate-polyelectrolyte (TDI-PE) scaffold are depicted in Fig. 6. The SEM analysis reveals an intricate network of interconnected structures, characterized by fibrous morphology, the scaffold exhibits a web-like architecture with fibers of varying diameters forming an irregular porous network, and the pore sizes and geometries within the structure show considerable variation, contributing to the scaffold's overall porosity,

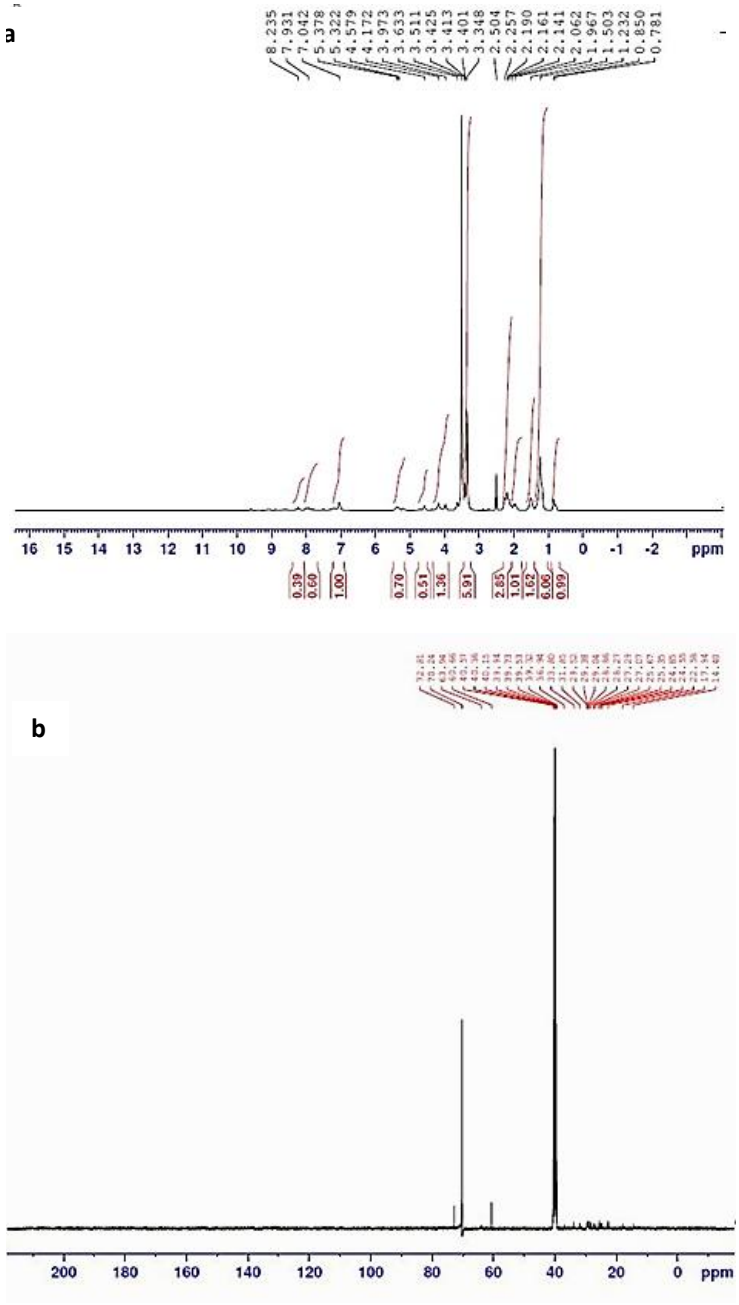

Fig. 9. a) X - 1H NMR spectrum of toluene diisocyanate with polyelectrolyte scaffold b) Y - 13C NMR spectrum of toluene diisocyanate with polyelectrolyte scaffold

the interconnected nature of these fibers results in highly porous and integrated architectural framework, potentially beneficial for cell infiltration, and nutrient transport in biological applications.

Nuclear Magnetic Resonance Spectroscopy Analysis

Nuclear magnetic resonance (NMR) spectroscopy was utilized to probe the chemical structure and composition of the synthesized scaffolds. Both 1H and 13C NMR analyses were performed on the toluene diisocyanate-graphene oxide (TDI-GO) and toluene diisocyanate-polyelectrolyte (TDI-PE) scaffolds.

The 1H and 13C NMR spectra of the TDI-GO scaffold are presented in Figs. 7a and 7b, respectively. The 1H NMR spectrum exhibits a cluster of intense signals in the range of 0.5-2.5 ppm, indicative of aliphatic protons. A notable peak at approximately 3.4 ppm is attributed to protons in proximity to electronegative moieties. The aromatic region, spanning 6.5-8 ppm, displays multiple peaks of moderate intensity. The ^{13}C NMR spectrum reveals strong signals between 10-40 ppm, corresponding to various aliphatic carbon environments. Signals in the 130-162 ppm range are characteristic of aromatic carbons, while a peak near 166 ppm suggests the presence of carbonyl functionalities.

Figs. 9a and 8b illustrate the 1H and 13C NMR spectra of the TDI-PE scaffold, respectively. The 1H NMR spectrum, spanning from -2 to 16 ppm, shows prominent signals between 1-2.5 ppm, attributed to protons adjacent to heteroatoms or functional groups. Multiple peaks in the 2-4 ppm range correspond to protons in diverse aliphatic environments. Low-intensity signals observed between 4.37-5.38 ppm are assigned to heteroatom-bound protons. The aromatic region (7-8 ppm) exhibits signals characteristic of aromatic protons. The 13C NMR spectrum, ranging from 0 to 220 ppm, features a prominent peak at approximately 40 ppm, indicative of aliphatic carbons. Multiple signals scattered between 20-80 ppm correspond to various aliphatic carbon environments, providing further insight into the scaffold's chemical structure.

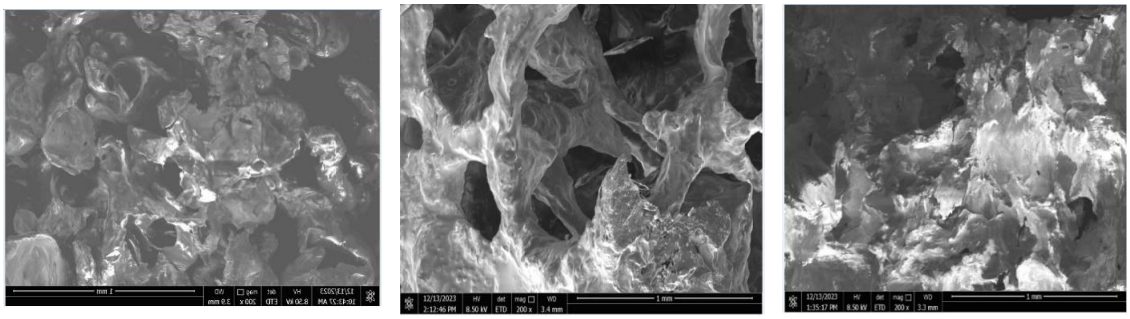

Fig. 10. Toluene diisocyanate with graphene oxide scaffold

Table 1. Porosity Quantification of Engineered Scaffolds

Scaffold Composition	$V_{initial}$ (mL)	V_{total} (mL)	$V_{residual}$ (mL)	Void Fraction (%)
Toluene-Drug Complex	10	12	4	75
Graphene Oxide-Toluene Hybrid	10	14	2	66
Toluene-Polyelectrolyte Blend	10	12	5	71

$V_{initial}$: Ethanol volume prior to scaffold submersion V_{total}: Aggregate volume post-submersion (ethanol + scaffold) $V_{residual}$: Remaining ethanol volume following scaffold extraction

Porosity Study

The structural void content of the fabricated scaffolds was assessed utilizing a liquid displacement technique, with ethanol serving as the displacement medium. Porosity values were determined by comparing the volume of ethanol retained within the scaffold matrix to the total volume encompassed by both the scaffold and ethanol. Table 1 presents the quantitative outcomes of this analysis.

The void fraction measurements ranged from 66% to 75%, indicating substantial porosity across all engineered scaffolds. The toluene-drug composite exhibited a 75% void fraction, while the graphene oxide-toluene hybrid displayed the lowest porosity at 66%, potentially attributable to the graphene oxide incorporation.

The elevated porosity observed in these scaffolds is paramount for diverse applications, including tissue engineering, controlled substance delivery, and filtration processes, highly porous architectures promote cellular infiltration, facilitate nutrient and metabolic waste exchange, and foster an environment conducive to tissue regeneration, the interconnected void network enables efficient loading and regulated release of therapeutic agents or bioactive molecules.

This porosity investigation demonstrates the successful engineering of highly porous scaffolds with variable void fractions contingent upon their compositional makeup. These findings offer critical insights into scaffolds' structural characteristics and illuminate their potential utility in biomedical and industrial domains.

Degradation Study of Prepared Scaffolds In Oxidation Solution

The degradation study of the prepared scaffolds in the oxidation solution exhibited distinct behaviors among the different scaffold compositions, decomposition was monitored using, Figs. 10 and 11.

SEM images during the oxidative degradation of prepared scaffolds

Based on the SEM images of the toluene with graphene oxide scaffold during oxidation degradation:

At 7 days, minimal degradation is observed, with the scaffold largely retaining its original structure. By 14 days, degradation becomes more apparent, with increased surface roughness and some erosion, though the overall architecture remains recognizable. At 21 days, significant degradation is visible, with extensive breakdown and larger pores forming throughout.

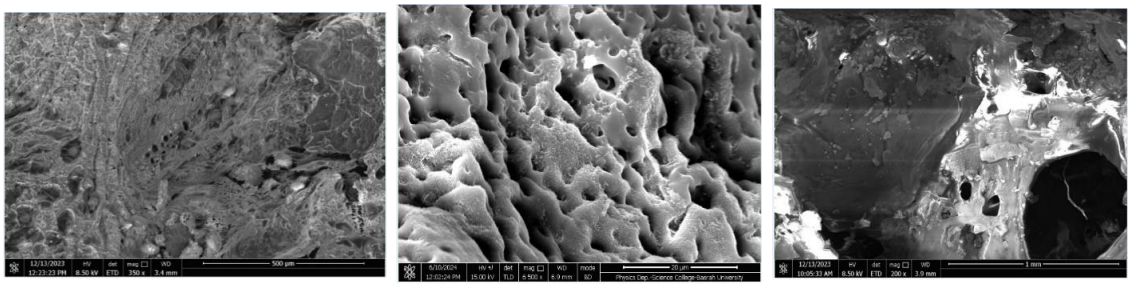

Fig. 11. Toluene diisocyanate with polyelectrolyte scaffold

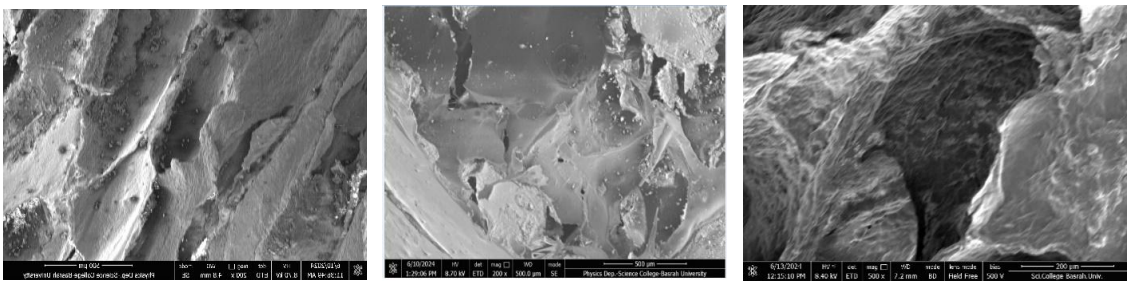

Fig. 12. Toluene with graphene oxide scaffold

This profile indicates a gradual, controlled degradation over several weeks in physiological conditions, potentially suitable for applications requiring sustained release or gradual tissue integration, the incorporation of polyelectrolytes offers tunable degradation properties for specific biomedical uses.

Based on images of SEM provided for toluene diisocyanate with polyelectrolyte scaffold during oxidation degradation:

At 7 days, initial signs of degradation are visible with minor surface roughening but the porous network remains largely intact, at 14 days, degradation is more pronounced, with increased roughness and porosity, some fibers show thinning or breakdown and larger voids are forming within the network, on 21 days, significant degradation is observed, original fibrous network is largely disrupted, with extensive breakdown of structure of scaffold, large pores and cavities are present, and some areas completely degraded.

This degradation profile suggests gradual breakdown of the scaffold over several weeks in physiological conditions, potentially suitable for controlled release applications, the incorporation of polyelectrolyte influenced the degradation rate and pattern, allowing for tunable properties, the scaffold demonstrates progressive erosion while maintaining some structural integrity through 21 day period.

In lysozyme Solution

prepared scaffold degradation behavior was evaluated at physiological conditions by immersing in a solution of lysozyme. Lysozyme is an enzyme present in various biological fluids and was employed to simulate the degradation process within the human body. Samples of each scaffold type were carefully weighed and immersed in individual containers filled with a phosphate-buffered saline (PBS) solution containing lysozyme at a pH of 7.4 and a temperature of 37°C (Figs. 12 and 13).

SEM images during the enzymatic degradation of prepared scaffolds

Based on the SEM images of the toluene with graphene oxide scaffold during enzymatic degradation:

At 7 days, initial signs of degradation are visible with minor surface roughening, but the porous network remains largely intact. By 14 days, degradation is more pronounced, with increased roughness and porosity, some fibers show thinning or breakdown, and larger voids are forming within the network. At 21 days, significant degradation is observed, the original fibrous network is largely disrupted, with an extensive breakdown of the scaffold structure, large pores and cavities are present and some areas are completely degraded.

This degradation profile suggests a gradual breakdown of the scaffold over several weeks in physiological conditions, potentially suitable for controlled release applications, the incorporation of graphene oxide influenced the degradation rate and pattern.

Based on the SEM images of the toluene diisocyanate with polyelectrolyte during enzymatic degradation:

At 7 days, initial signs of degradation are visible with minor surface roughening, but the porous network remains largely intact. By 14 days, degradation is more pronounced, with increased roughness and porosity. Some fibers show thinning or breakdown and larger voids are forming within the network. At 21 days, significant degradation is observed, the original fibrous network is largely disrupted, with an extensive breakdown of the

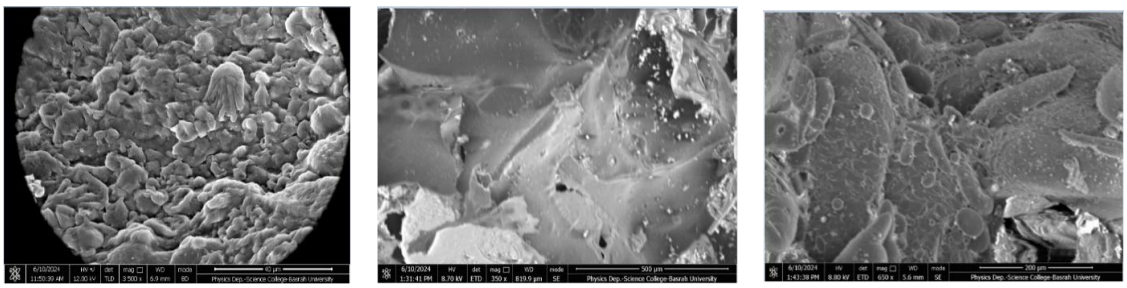

Fig. 13. Toluene diisocyanate with polyelectrolyte scaffold

scaffold structure, large pores and cavities are present and some areas are completely degraded.

This degradation profile suggests a gradual breakdown of the scaffold over several weeks in physiological conditions, suitable for controlled release applications, the incorporation of graphene oxide influenced the degradation rate and pattern.

These findings highlight the influence of the scaffold composition on their degradation behavior in the presence of enzymes mimicking the physiological environment, the incorporation of graphene oxide and the selection of different isocyanate components played a role in modulating the degradation rates, offering potential avenues for tailoring the scaffold properties for specific biomedical applications.

In Vivo Analysis of TDI-Based Scaffolds

The in vivo evaluation of TDI-based scaffolds incorporated with polyelectrolyte/Icariin (TDI / PE / I) and graphene oxide/Icariin (TDI/GO/I) was conducted through implantation in rabbit over four-week period. Hematological and biochemical parameters were monitored to assess scaffolds' biocompatibility and potential systemic effects.

The hematological analysis revealed dynamic changes in blood cell populations across both experimental groups, the TDI/PE/I group demonstrated progressive increase in red blood cell (RBC) count from $3.32 \pm 0.13 \times 10^{12}$/L in one week to peak of $5.27 \pm 0.4 \times 10^{12}$/L by week three, followed by slight decline to $4.27 \pm 0.53 \times 10^{12}$/L on week four, this pattern was accompanied by corresponding changes in levels of hemoglobin (HGB) and hematocrit (HCT), suggesting active erythropoiesis during the healing process. The TDI/GO/I group exhibited different pattern, with more moderate fluctuations in RBC counts ranging from 3.09 ± 0.83 to $4.52 \pm 0.37 \times 10^{12}$/L throughout the study period.

White blood cell (WBC) responses indicated initial inflammatory phase followed by resolution. Both scaffold groups showed elevated WBC counts in the first two weeks (TDI/PE/I: 18.8 ± 3.66 to $20.24 \pm 1.8 \times 10^{9}$/L; TDI/GO/I: 17.73 ± 1.06 to $17.83 \pm 2.31 \times 10^{9}$/L) that gradually normalized by week four. The differential WBC analysis revealed that granulocytes (GRA) were the predominant cell type during the initial response, suggesting appropriate acute inflammatory reaction to the implanted materials.

Platelet (PLT) counts showed notable variations between the groups, with TDI/PE/I exhibiting wider fluctuations (211.67 ± 391.28 to $242 \pm 18.08 \times 10^{9}$/L) compared to TDI/GO/I (131.67 ± 14.57 to $253.33 \pm 69.18 \times 10^{9}$/L). These variations remained within physiologically acceptable ranges and indicated normal hemostatic function throughout the healing process.

Liver function markers showed distinct patterns between the scaffold types, the TDI/PE/I group demonstrated initially elevated ALT levels (158 ± 52.12 U/L) that decreased and stabilized by week two, while AST levels fluctuated moderately. In contrast, the TDI/GO&I group maintained more consistent ALT levels but showed variable AST activity. Alkaline phosphatase (ALP) levels in both groups suggested active bone remodeling, with the TDI/PE/I group showing a progressive increase from 49.33 ± 7.51 U/L to 129 ± 3.61 U/L by week three.

Protein metabolism parameters, including total protein (TP) and albumin (ALB), remained relatively stable in both groups, though slightly lower than the negative control, possibly indicating mild systemic adaptation to the implanted materials. Calcium and phosphorus levels, crucial for bone metabolism, showed minimal variations from physiological ranges, suggesting maintained mineral homeostasis.

When we compared with control groups, scaffold types demonstrated favorable biocompatibility profiles, the positive control group showed similar trends in inflammatory markers and bone metabolism parameters, while the negative control maintained baseline values through the study period. The TDI/PE&/I group exhibited slightly more pronounced initial inflammatory responses but better stabilization of hematological parameters by week four.

These findings suggest both TDI-based scaffold formulations are biocompatible and support tissue regeneration, with some variations in their systemic effects, the TDI/PE/I scaffold showed more dynamic responses in hematopoietic and bone metabolism markers, while the TDI/GO/I scaffold demonstrated more moderate but consistent biological responses, the observed parameters remained within acceptable physiological ranges, indicating the safety of both scaffold types for potential clinical applications.

Radiographic examination revealed distinct healing patterns between TDI/PE/I and TDI/GO/I scaffolds over the four-week implantation period,

Fig. 9. In the first week post-implantation, both scaffold groups exhibited radiolucent areas at the defect site with notable periosteal reaction at the hole margins, indicating the initial hematoma formation and recruitment of inflammatory mediators. This early response reflected the onset of the healing cascade and cellular infiltration at the implantation site.

By week two, the healing trajectories of the two scaffolds began to diverge significantly. The TDI/GO/I group demonstrated marked progression, characterized by increased opacity and initial marginal union at the defect site, suggesting active-matrix deposition and the transition into the inflammatory phase. In contrast, the TDI/PE/I group maintained radiolucent characteristics similar to the first week, indicating a more gradual progression through the early healing stages.

Week three revealed more pronounced differences between the two scaffold types. TDI/GO/I implants exhibited substantial advancement in the healing process, achieving the semi-complete union of the defect margins. What we observed suggested successful progression through the soft callus formation stage and the initiation of ossification. The TDI/PE/I group,

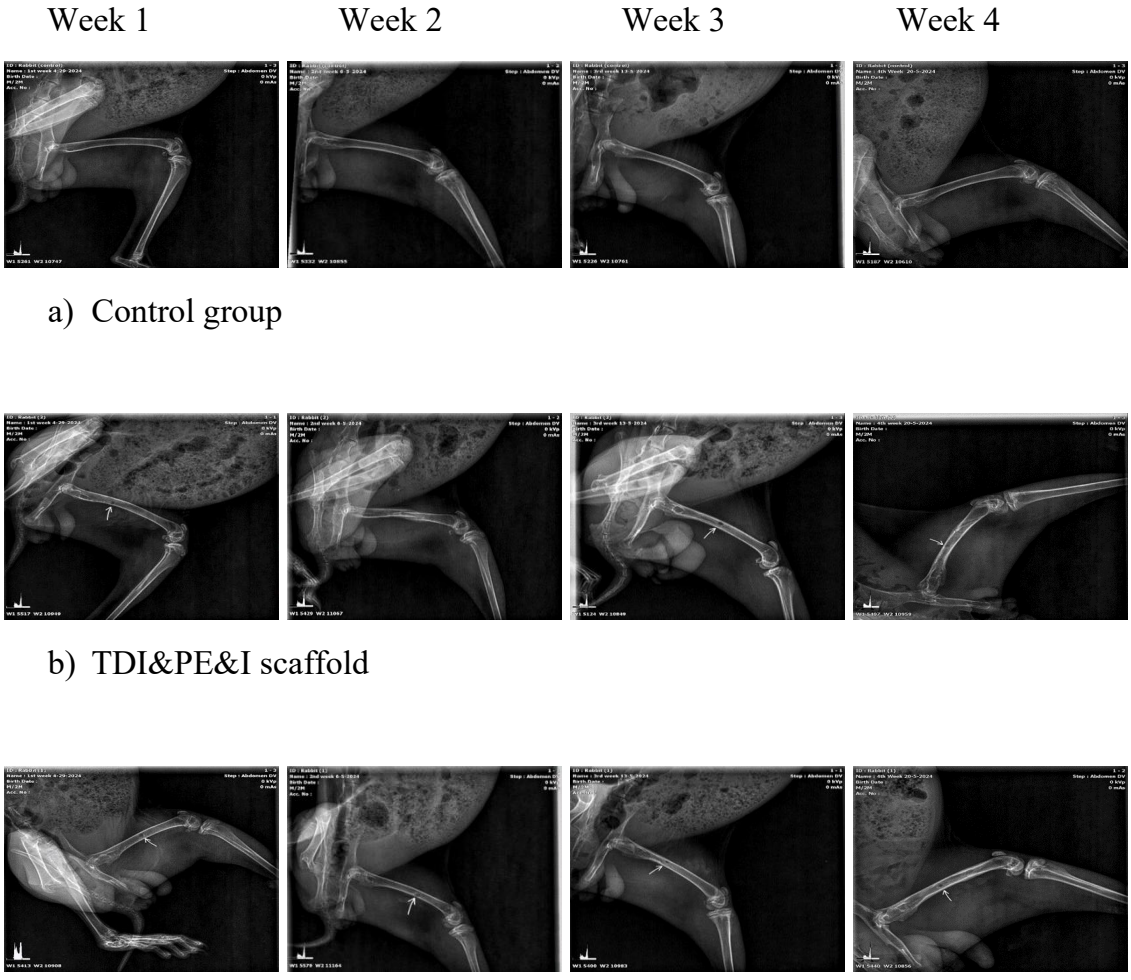

Fig. 14. Radiographic progression of bone healing in scaffold-implanted defects: (a) Control group showing normal bone structure; (b) TDI&PE&I scaffold group demonstrating gradual healing with persistent radiolucency through weeks 1-3 and partial union by week 4; (c) TDI&GO&I scaffold group exhibiting progressive opacity and achieving semi-complete union by week 3-4, indicating enhanced bone regeneration.

however, continued to show radiolucent areas at the implantation site with persistent periosteal reaction, indicating a delayed progression through the healing cascade.

By week four, the TDI/GO/I scaffold demonstrated superior healing outcomes, maintaining the semi-complete union observed in the previous week with enhanced matrix mineralization. The TDI/PE/I group showed improved radiographic features compared to earlier weeks, with increased opacity and partial union at the defect margins, though not achieving the same degree of healing as the TDI/GO/I grou (Fig. 14).

These radiographic findings suggest that the incorporation of graphene oxide in TDI/GO/I scaffold potentially enhanced the bone healing process, facilitating more rapid progression through the healing stages compared to polyelectrolyte-containing TDI/PE/I scaffold, the observed differences in healing patterns attributed to the unique structural and biological properties of graphene oxide, which influence cellular response and matrix organization during bone regeneration.

Spectroscopic analysis through FTIR provided crucial insights into the chemical composition of both microspheres and scaffolds. The identification of characteristic peaks corresponding to C-O stretching (1007.78 cm^{-1}), C-N bending (1264 cm^{-1}), and N-H stretching (3406 cm^{-1}) confirms the successful synthesis and integration of the desired functional groups. The presence of amide-related peaks at 1609 cm^{-1} and 1665 cm^{-1} particularly indicates the formation of stable chemical bonds essential for controlled degradation and drug release.

The XRD analysis revealed notable crystalline features, with the peak at 2θ of 20.66° (d-spacing 4.30 Å) indicating organized structural domains within the polyurethane component. Additional peaks at 11.69°, 23.48°, and 63.32° demonstrate the successful incorporation of polyelectrolyte components, contributing to the scaffold's overall structural stability and functionality.

The scaffold's morphological characteristics, as revealed by SEM analysis, demonstrate sophisticated interconnected network of pores with varying geometries. This feature proves advantageous for multiple reasons: it enhances surface area for drug distribution, facilitates cellular attachment and migration and enables efficient nutrient transport throughout the scaffold matrix, the observed gradual degradation pattern in the two oxidative and enzymatic conditions over 21 days suggests controlled breakdown mechanism suitable for sustained drug release applications.

The porosity analysis revealed intriguing trends, with values ranging from 70% to 91% depending on scaffold composition, the systematic decrease in porosity following the incorporation of hydroxyapatite and Icariin microspheres aligns with theoretical predictions while maintaining sufficient void space for cellular activities, and drug diffusion, this balance between component integration and preserved porosity underscores the scaffold's potential for combined drug delivery, and tissue engineering applications.

The degradation studies in both oxidative and enzymatic environments provided valuable insights into the scaffold's stability under physiological conditions. The progressive structural changes observed through SEM imaging over 21 days demonstrate a controlled degradation process that potentially matches tissue regeneration rates in vivo. The influence of polyelectrolyte components on degradation patterns suggests possible mechanisms for tuning scaffold breakdown rates to meet specific therapeutic requirements.

These findings collectively demonstrate the sophisticated interplay between scaffold composition, structure, and function, highlighting the potential of these systems for advanced biomedical applications. The combination of controlled drug release capabilities, optimized porosity, and tunable degradation characteristics positions these scaffolds as promising candidates for targeted drug delivery and tissue engineering applications.

in vivo, studies revealed fascinating insights into the biological response to our scaffolds. The TDI/GO/I scaffold showed particularly encouraging results, with radiographic evidence suggesting faster bone regeneration compared to TDI/PE/ I variants. Blood analysis for the week four period showed both scaffold types maintained acceptable biocompatibility profiles, though the TDI/GO/I group demonstrated more stable hematological parameters, the gradual decrease in white blood cell counts after initial elevation suggests normal inflammatory response followed by successful resolution. Liver function markers, while showing some early fluctuations, stabilized within normal ranges by the study's end. The progressive increase

in alkaline phosphatase levels, particularly in the TDI/GO/ I group, indicates active bone formation at the implant site. Radiographic examination revealed that by week three, the TDI/GO/ I scaffolds achieved notable defect closure with visible matrix mineralization, while TDI/PE/ I scaffolds showed a more gradual healing pattern. The integration of graphene oxide appears to enhance the scaffold's osteogenic potential, possibly due to its unique surface properties and ability to support cell adhesion. These findings align with the observed porosity and degradation characteristics, where the maintained structural integrity over several weeks provided an optimal environment for tissue ingrowth, the balanced inflammatory response, and sustained healing progression demonstrate that our scaffold design successfully bridges the gap between material stability and biological integration.

Comparison with Recent Studies

In comparison with recent studies in the field, our findings demonstrate both similarities and unique characteristics. The work of [11] exploring sodium alginate/chitosan polyelectrolyte microparticles showed parallel trends in controlled release behavior, though with different therapeutic agents. While their study focused on rifampicin release from polyelectrolyte matrices, our investigation of Icariin demonstrated comparable sustained release patterns over 24 hours. However, our scaffold systems exhibited more pronounced control over initial burst release, particularly in the M1 formulation (0.01g drug loading), suggesting potential advantages in maintaining therapeutic concentrations.

The structural characteristics of our scaffolds align with the broader trends identified in [12] comprehensive review of polymeric materials in tissue engineering. Their analysis highlighted the importance of interconnected porosity for successful tissue integration, which our scaffolds achieved with void fractions ranging from 66% to 75%. Notably, our toluene-drug complex scaffold demonstrated superior porosity (75%) compared to typical ranges reported in their review, potentially offering enhanced cellular infiltration and nutrient transport capabilities.

The incorporation of graphene oxide in our TDI-GO scaffold resulted in unique structural and functional properties not observed in conventional polyelectrolyte systems described by [11] while their work emphasized the role of polyelectrolyte interactions in drug delivery, our dual-component approach combining graphene oxide with toluene diisocyanate achieved enhanced mechanical stability and controlled degradation profiles. The findings suggest advantages in applications requiring prolonged structural support during tissue regeneration.

This comparative positions our scaffold as promising to biomedical applications, offering advancements in controlled drug delivery, structural stability, and tissue integration capabilities, the observed performance characteristics, particularly in terms of degradation control, and in vivo response, represent meaningful progress in addressing key challenges identified in recent literature regarding scaffold-based tissue engineering approaches.

CONCLUSION

The evaluation of our polymeric scaffolds with Icariin-loaded sodium alginate nanospheres yielded promising results in multiple assessment criteria. Our chemical analysis confirmed successful component integration, while microscopic examination revealed an interconnected porous structure crucial for cellular interactions, the scaffolds demonstrated controlled drug release through 24 hours, with release rates effectively modulated through drug loading. The scaffolds maintained high porosity (70-91%) even after incorporating additional components. The in vivo studies provided compelling evidence of their therapeutic potential, with both scaffold variants showing good biocompatibility in rabbit models, the TDI/GO/I scaffold particularly excelled, demonstrating enhanced bone regeneration and stable hematological profiles over the four-week implantation period, radiographic analysis revealed progressive bone formation, with significant defect closure observed by week three, while blood parameters remained within normal ranges throughout the study, the controlled degradation patterns observed both in vitro and in vivo support their suitability for clinical applications, these findings demonstrate that our scaffold system offers versatile platform for drug delivery and tissue regeneration, with tunable properties that adapted to specific therapeutic needs, the successful in vivo performance, combined with controllable drug release and degradation characteristics, suggests significant

potential for clinical translation in orthopedic and drug delivery applications.

CONFLICT OF INTEREST

The authors declare that there is no conflict of interests regarding the publication of this manuscript.

REFERENCES

1. Adepu S, Ramakrishna S. Controlled Drug Delivery Systems: Current Status and Future Directions. Molecules (Basel, Switzerland). 2021;26(19):5905.
2. Thang NH, Chien TB, Cuong DX. Polymer-Based Hydrogels Applied in Drug Delivery: An Overview. Gels (Basel, Switzerland). 2023;9(7):523.
3. Terzopoulou Z, Zamboulis A, Koumentakou I, Michailidou G, Noordam MJ, Bikiaris DN. Biocompatible Synthetic Polymers for Tissue Engineering Purposes. Biomacromolecules. 2022;23(5):1841-1863.
4. Radulescu D-M, Neacsu IA, Grumezescu A-M, Andronescu E. New Insights of Scaffolds Based on Hydrogels in Tissue Engineering. Polymers. 2022;14(4):799.
5. Sharma D, Saha S, Satapathy BK. Recent advances in polymer scaffolds for biomedical applications. J Biomater Sci Polym Ed. 2021;33(3):342-408.
6. Braun H. Methylene Diphenyl Diisocyanate (MDI) and Toluene Diisocyanate (TDI). Industrial Arene Chemistry: Wiley; 2023. p. 1525-1574.
7. Azarmgin S, Torabinejad B, Kalantarzadeh R, Garcia H, Velazquez CA, Lopez G, et al. Polyurethanes and Their Biomedical Applications. ACS Biomaterials Science & Engineering. 2024;10(11):6828-6859.
8. Zare P, Aleemardani M, Seifalian A, Bagher Z, Seifalian AM. Graphene Oxide: Opportunities and Challenges in Biomedicine. Nanomaterials (Basel, Switzerland). 2021;11(5):1083.
9. Eivazzadeh-Keihan R, Sadat Z, Lalebeigi F, Naderi N, Panahi L, Ganjali F, et al. Effects of mechanical properties of carbon-based nanocomposites on scaffolds for tissue engineering applications: a comprehensive review. Nanoscale advances. 2023;6(2):337-366.
10. Municoy S, Álvarez Echazú MI, Antezana PE, Galdopórpora JM, Olivetti C, Mebert AM, et al. Stimuli-Responsive Materials for Tissue Engineering and Drug Delivery. Int J Mol Sci. 2020;21(13):4724.
11. Hussein Al-Assady NA, Badran HA, Kamil SA, Abo-Alhal RC. Preparation and evaluation in vitro release of sodium alginate/chitosan polyelectrolyte microparticles containing rifampicin and theoretical study using DFT methods. Journal of Biomolecular Structure and Dynamics. 2023;42(4):1795-1811.
12. Socci MC, Rodríguez G, Oliva E, Fushimi S, Takabatake K, Nagatsuka H, et al. Polymeric Materials, Advances and Applications in Tissue Engineering: A Review. Bioengineering (Basel, Switzerland). 2023;10(2):218.